Band structure and ordering of magnetic superlattices

1990 J. Phys.: Condens. Matter 2 4197

(http://iopscience.iop.org/0953-8984/2/18/016)

J. Phys.: Condens. Matter **2** (1990) 4197–4208. Printed in the UK

Band structure and ordering of magnetic superlattices

W M Fairbairn and S Y Yip
Department of Physics, University of Lancaster, Lancaster LA1 4YB, UK

Received 18 August 1989, in final form 28 December 1989

Abstract. The unit cell of a superlattice which contains two multiplane layers corresponding to two different constituent atoms, one of which is a long-range magnetic rare-earth metal, is represented along the superlattice direction by square-well potentials of appropriate depths. The electronic band structure of this bilayer is obtained numerically. The variation in charge density within the bilayer is discussed. The information so obtained allows also the magnetic ordering of the superlattice system to be determined by establishing the variation in the RKKY exchange interaction with distance. Results for this simple model show encouraging agreement with experimental evidence that the type of ordering is affected by the thickness of the magnetically inert multiplane layer and that long-range magnetic coherence may exist in these structures.

1. Introduction

Now that highly perfect single-crystal rare-earth (RE) superlattices can be successfully grown using the MBE method, much experimental work has been done to investigate the magnetic properties of such structures (Rhyne *et al* 1989). A magnetic superlattice typically consists of L bilayers of N atomic planes of a long-range magnetic RE metal A followed by M such planes of a non-magnetic element B and is denoted by $(A_N\text{–}B_M)_L$. Most experiments have been performed with at least 100 bilayers each containing 20–50 planes. Although such a system is three dimensional, it is its characteristic properties in the direction normal to the plane surface of the material on which it has been deposited that are of prime interest. It has been found by x-ray diffraction (Borchers *et al* 1987) and neutron diffraction techniques (Majkrzak *et al* 1987, Rhyne *et al* 1987, Majkrzak 1989) that the magnetisation of these compounds can exhibit long-range coherence across the magnetically inert layers, and that the thickness of these layers has a profound effect on the magnetic ordering (Majkrzak *et al* 1988, Hong *et al* 1987). The question that one asks then is whether the RKKY indirect-exchange interaction (Kittel 1963), which is so successful in accounting for the magnetic behaviour of pure RE metals and alloys, is responsible also for these observed magnetic effects. Here a theoretical approach to the question is provided through the analysis of a simple model which examines the properties of the non-localised electrons particularly along the direction of the c axis of the HCP structure of the superlattice. Numerical calculation establishes the band structure associated with such a system and provides information about how the electron distribution can vary within the bilayers. It provides also a basis for establishing how the long-range character of the RKKY coupling associated with the magnetic

0953-8984/90/184197 + 12 $03.50

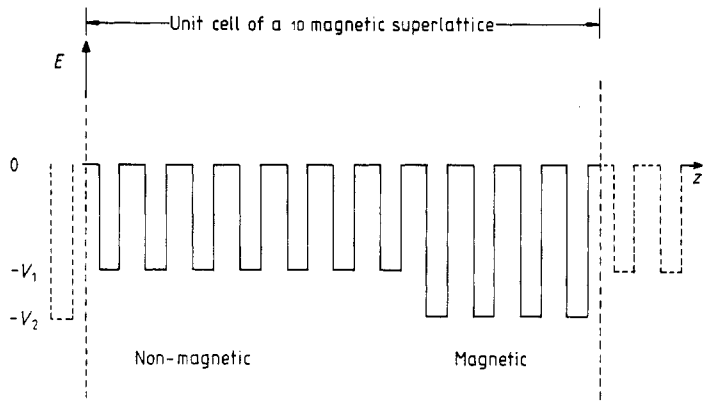

Figure 1. The unit cell of the 1D magnetic superlattice is represented by square wells of depths V_1 and V_2 along the superlattice direction. The width of the two types of well is b with spacing a between them. V_1 and V_2 are chosen such that there are three bound states in the wells representing the non-magnetic atoms and four bound states in those representing the magnetic ones. The top energy levels $E_1^{(3)}$ and $E_2^{(4)}$ corresponding to V_1 and V_2, respectively, are chosen to be at approximately the same energy. In this example there are $N = 7$ wells of depth V_1 followed by $M = 4$ wells of depth V_2.

element varies when different thicknesses of the non-magnetic material are incorporated in the bilayer.

2. The model

In the model the two types of atom in the superlattice are represented by square wells of different depth, so that there are N wells of depth V_1, followed by M wells of depth V_2. This basic unit cell, i.e. one bilayer, is then repeated so that the structure as a whole is periodic with periodicity $(N+M)(a+b)$, where a is the spacing between wells and b the width of the wells, taken for simplicity to be the same for both atoms (see figure 1). For our purposes, because it is important to identify clearly the number and position of the bound states at each atomic site, the limiting case of δ-wells is inappropriate. The depth of the wells are chosen such that they provide energy levels which are appropriate for the elements involved, and that the top levels E_1^1 and E_2^1 corresponding to the potential depths V_1 and V_2, respectively, are at approximately the same energy. Their values were determined numerically in accordance with the solution for a single square well of depth V and width b which is given by

$$p(\varepsilon) \text{ or } q(\varepsilon) = \sqrt{mVb^2/2\hbar^2 - \varepsilon^2}$$

where $p(\varepsilon) = \varepsilon \tan \varepsilon$ and $q(\varepsilon) = -\varepsilon \cot \varepsilon$ with

$$\varepsilon = \sqrt{mEb^2/2\hbar^2}.$$

For an electron of energy E in the unit cell, the Schrödinger equation has the solutions

$$A_r \exp(-\gamma z) + B_r \exp(\gamma z)$$

in regions of zero potential, $r = 0, 2, 4, \ldots, 2(N+M)$

$A_r \exp(i\beta_1 z) + B_r \exp(-i\beta_1 z)$

in regions of potential $-V_1$, $r = 1, 3, 5, \ldots, (2N-1)$

$A_r \exp(i\beta_2 z) + B_r \exp(-i\beta_2 z)$

in regions of potential $-V_2$, $r = (2N+1), (2N+3), \ldots, 2(N+M)-1$

where

$$(i\gamma)^2 = 2mE/\hbar^2$$

$$\hbar^2\beta_1^2 = 2m(E + V_1)$$

$$\hbar^2\beta_2^2 = 2m(E + V_2).$$

By requiring that the wavefunction satisfies the necessary boundary conditions whenever the potential changes, a relationship between the coefficients of the wavefunctions (A_0, B_0) and $(A_{2(N+M)}, B_{2(N+M)})$ can be obtained, i.e.

$$\begin{bmatrix} A_{2(N+M)} \exp[-\gamma(a+b)(N+M)] \\ B_{2(N+M)} \exp[\gamma(a+b)(N+M)] \end{bmatrix} = \mathbf{R}^M \mathbf{Q}^N \begin{bmatrix} A_0 \\ B_0 \end{bmatrix}$$

where

$$\mathbf{Q} = \begin{bmatrix} \exp(-\gamma a)\left(\cos(\beta_1 b) + \dfrac{\beta_1^2 - \gamma^2}{2\gamma\beta_1}\sin(\beta_1 b)\right) & \dfrac{\beta_1^2 + \gamma^2}{2\gamma\beta_1}\sin(\beta_1 b) \\ -\dfrac{\beta_1^2 + \gamma^2}{2\gamma\beta_1}\sin(\beta_1 b) & \exp(\gamma a)\left(\cos(\beta_1 b) - \dfrac{\beta_1^2 - \gamma^2}{2\gamma\beta_1}\sin(\beta_1 b)\right) \end{bmatrix}$$

and $\mathbf{R}$ is the same as $\mathbf{Q}$ but with β_1 replaced by β_2. In order to pass from one end of the superlattice bilayer to the other to obtain $(A_{2(N+M)}, B_{2(N+M)})$, one must operate on (A_0, B_0) with the 2×2 matrix $\mathbf{T} = \mathbf{R}^M\mathbf{Q}^N$. Further, by Bloch's theorem, this operation must be equivalent to operating with the matrix

$$\begin{bmatrix} \exp[ik_z(N+M)(a+b)] & 0 \\ 0 & \exp[ik_z(N+M)(a+b)] \end{bmatrix}$$

$$= \exp[ik_z(N+M)(a+b)]\, I_2 = \kappa I_2$$

so that

$$\mathbf{T}\begin{bmatrix} A_0 \\ B_0 \end{bmatrix} = \kappa I_2 \begin{bmatrix} A_0 \\ B_0 \end{bmatrix} \tag{1}$$

giving

$$\det(\kappa I_2 - \mathbf{T}) = 0$$

if solutions are to exist. Since $\det \mathbf{T}$ equals unity, it can be written as

$$\cos[k_z(N+M)(a+b)] = \tfrac{1}{2}\operatorname{Tr}\mathbf{T}. \tag{2}$$

This is the fundamental equation which enables us to determine numerically the band structure of the superlattice with the energy E of the electron being a function of wavenumber k_z. It will further allow the charge density across the unit cell to be computed

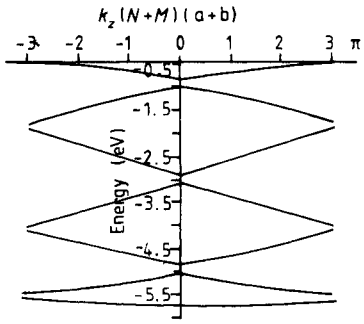

Figure 2. Band structure of the $N = 3$, $M = 4$ superlattice unit cell when E_1^3 and E_2^4 are at about -3.7 eV.

and, with the information so obtained, we can also investigate how the RKKY exchange interaction varies with distance.

3. Band structure

The parameters needed for the computation are the values of N, M, V_1, V_2, a and b. For convenience, a and b are taken to be identical (and equal to 1.5 Å), but V_1 and V_2 are chosen so as to permit the existence of three bound states in the wells representing the non-magnetic atom and four bound states in those representing the magnetic ones. We have also fixed M to have the values 3 and 4, with N varying from 3 up to 17. The two different types of atom are each assumed to contribute one electron to the conduction band so that, when $N + M$ is an odd number and with spin being taken into account, the conduction band is half filled. It has been found for our simple model that in the energy region of interest, i.e. near the top energy level, for appropriate values of V_1 and V_2 there appear $N+M$ bound sub-bands which are very close together when the top energy levels $E_1^{(3)}$ and $E_2^{(4)}$ corresponding to the potentials V_1 and V_2, respectively, are approximately the same, indicating almost complete non-localisation of the wave functions across the whole unit cell as one might expect. However, if E_1^3 and E_2^4 differ slightly, then the resulting energy bands have wider gaps between them and consequently some states are localised within the unit cell. These features are illustrated in figure 2 and figure 3. Note that in both cases the bottom bands are very narrow, showing that the electrons there are more tightly bound.

4. Charge distribution

The electron probability distribution across the superlattice bilayer can be obtained using the relations

$$\int_{z_1}^{z_2} \psi_r \psi_r^* \, \mathrm{d}z = \frac{\sinh(\gamma a)}{\gamma}(|A_r \exp(-\gamma z_0)|^2 + |B_r \exp(\gamma z_0)|^2) + (A_r B_r^* + B_r A_r^*)a$$

in the regions of zero potential with $r = 0, 2, 4, \ldots, 2(N + M)$, where z_0 is the midpoint of the barrier in question. Also in the potential wells, we have

$$\int_{z_1}^{z_2} \psi_r \psi_r^* \, \mathrm{d}z = b(|A_r|^2 + |B_r|^2) + \frac{\sin(\Omega b)}{\Omega} \times [A_r B_r^* \exp(\mathrm{i}2\Omega z_0') + A_r^* B_r \exp(-\mathrm{i}2\Omega z_0')]$$

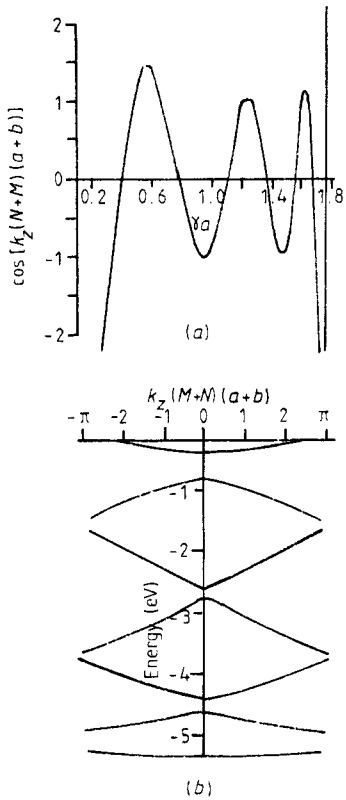

Figure 3. (*a*) The slight difference in the top energy levels E_1^3 and E_2^4 results in the sub-bands having wider band gaps. Here $E_1^{(3)} \simeq -3.51$ eV, $E_2^{(4)} \simeq -3.75$ eV with $N = 3$, $M = 4$. (*b*) The dispersion relation shows for these values of the parameters that part of the function $\frac{1}{2}$ Tr **T** which appears on the RHS of (2) and which is relevant for the least-tight sub-bands shown in the accompanying diagram.

with $r = 1, 3, 5, \ldots, 2(N + M) - 1$, where $\Omega = \beta_1$ or β_2 and z_0' is the midpoint of the associated well. The coefficients (A_r, B_r), which are complex, are obtained as follows. From (1), we have

$$\begin{bmatrix} \kappa - T_{11} & -T_{12} \\ -T_{21} & \kappa - T_{22} \end{bmatrix} \begin{bmatrix} A_0 \\ B_0 \end{bmatrix} = 0.$$

This gives

$$\begin{bmatrix} A_0 \\ B_0 \end{bmatrix} \equiv \begin{bmatrix} T_{12} \\ \kappa - T_{11} \end{bmatrix}.$$

This relation allows the various A_r and B_r to be determined since these can be expressed in terms of (A_0, B_0) through the matrices **R** and **Q**, thus enabling the electron probability distribution across the superlattice bilayer to be found. Results for the $N = 9$, $M = 4$ unit cell when E_1^3 and E_2^4 are at about -3.7 eV show that in general the charge density is distributed non-uniformly at the band edges but tends to be more or less uniform at the middle of the higher bands, while the distribution for the bottom bands tends to be very much the same for most states within the particular band with perhaps a little spreading as one goes from the bottom to the top of the band. Figure 4 shows the charge distribution for bands 1, 3 and 7 for the particular unit cell considered. As can be seen, the charge density is higher in some regions than in others for the narrower bottom bands, indicating that the electron is more likely to be found in these regions of the

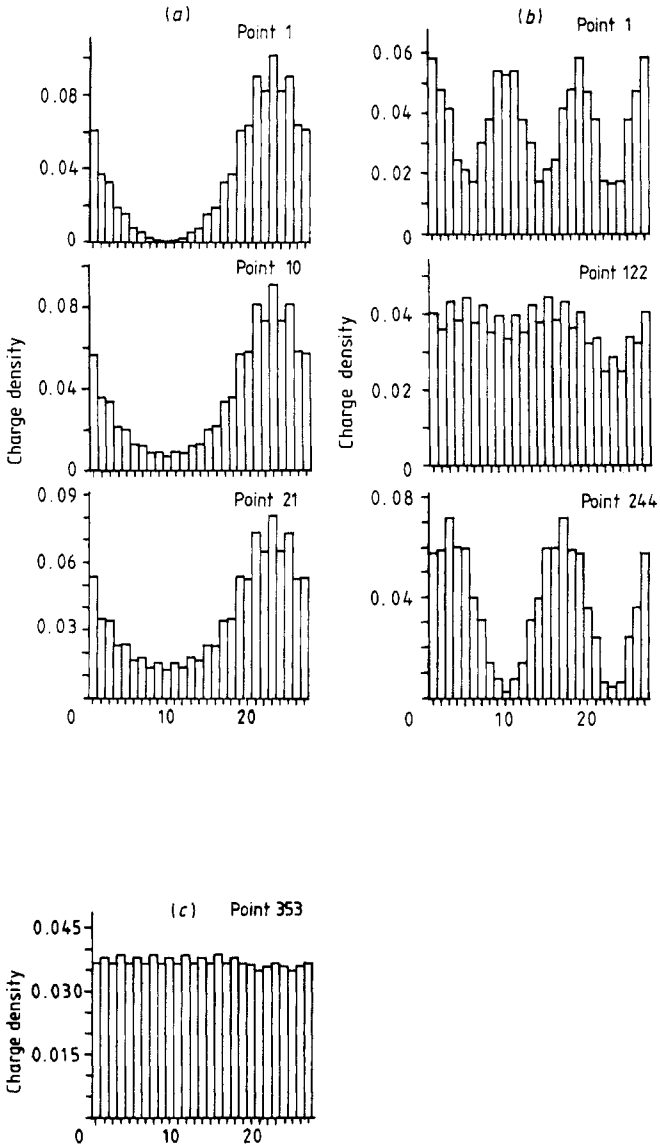

Figure 4. Electron distributions within bands 1, 3 and 7 for the $N = 9$, $M = 4$ superlattice bilayer when $E_1^{(3)}$ and $E_2^{(4)}$ are at about -3.7 eV. The abscissa is in direction of increasing n where n is related to z by

$$z = (n-1)(a+b)/2$$
$$n = 1, 2, 3, \ldots, 2(N+M)+1$$

so that, when n is odd, z is the midpoint of the associated barrier, while n even corresponds to when z is the midpoint of a potential well. (*a*) The charge density for states chosen from three bands are shown. For band 1, the lowest in energy, the electron for the three states chosen is seen to be more localised in some regions of the bilayer than in others. (*b*) The same applies to band 3 but now a more uniform distribution for the states in the middle of the band begins to occur. (*c*) For band 7, in which the Fermi energy lies for this particular unit cell, there is an almost uniform distribution throughout the band except at the band edges; the distribution shown relates to a state near the middle of the band.

unit cell. For the wider higher bands, however, the charge density is quite uniformly distributed showing that there is equal probability of finding the electron anywhere in the superlattice unit cell.

5. RKKY exchange interaction

The model as it stands can represent any superlattice that one cares to choose, and not just magnetic superlattices. For it to be a magnetic superlattice the atoms representing the magnetic element must possess magnetic moments such that they could interact to

produce the observed magnetic properties in these structures. Magnetic moments of the RE arise from the localised spins corresponding to their unfilled 4f shells (Cooper 1972). Since overlap with neighbouring atoms in the lattice is small, one would not normally expect cooperative magnetic phenomena in these materials to occur. The fact that they do is explained by the RKKY exchange interaction (Kittel 1963) in which neighbouring ions interact indirectly via the conduction electrons contributed by the 5d and 6s levels. The form of the interaction in three dimensions using free-particle wavefunctions $\exp(i\boldsymbol{k}\cdot\boldsymbol{r})$ is given by

$$H''(\boldsymbol{x}) = \frac{\boldsymbol{I}_n \cdot \boldsymbol{I}_m}{2} \frac{m^* J^2}{(2\pi)^6} P \int_0^{k_F} d^3k \int_{k_F}^{\infty} d^3k' \frac{\exp[-i(\boldsymbol{k}-\boldsymbol{k}')\cdot\boldsymbol{x}]}{k^2 - k'^2} + CC$$

where

$$J = \int d^3x\, \psi_{k'}^*(\boldsymbol{x}) A(\boldsymbol{x}) \psi_k(\boldsymbol{x})$$

$A(\boldsymbol{x})$ normally being chosen to be a delta function; $\boldsymbol{I}_n$ is the spin associated with the ion at site n, and $\boldsymbol{x}$ is the distance between the spins at sites n and m. Upon performing the integration for a spherical Fermi surface, this expression reduces to a simple analytic form, i.e.

$$H''(\boldsymbol{x}) = \boldsymbol{I}_n \cdot \boldsymbol{I}_m [4J^2 m^*/(2\pi)^3] k_F^4 F(2k_F r)$$

where $r = |\boldsymbol{x}|$ and

$$F(2k_F r) = [2k_F r \cos(2k_F r) - \sin(2k_F r)]/(2k_F r)^4.$$

For our model where the wavefunction is of the form indicated earlier whose coefficients are complex, such a simple analytical expression for the exchange interaction is not possible. In three dimensions the interaction for the superlattice takes the form

$$H''(\boldsymbol{x}) = \frac{\boldsymbol{I}_n \cdot \boldsymbol{I}_m}{2} \frac{J^2}{(2\pi)^6} P \iint \frac{\psi_n^*(\boldsymbol{k})\psi_m(\boldsymbol{k})\psi_n(\boldsymbol{k}')\psi_m^*(\boldsymbol{k}')}{E_k - E_{k'}} d\boldsymbol{k}\, d\boldsymbol{k}'$$

where the ψ_i are the wavefunctions associated with the potential wells corresponding to the magnetic atoms, E_k is given by $(\hbar^2/2m)\ (k_x^2 + k_y^2 + \beta_2^2)$ and is measured from the bottom of the wells. Using cylindrical polar coordinates (K, k_z, θ) with $\psi(\boldsymbol{k}) \sim \exp(ik_x x)$ $\exp(ik_y y)\ \psi(\beta_2(k_z), z)$, the integral can be written after performing the angular integration as

$$H''(\boldsymbol{x}) = (2\pi)^2 \frac{\boldsymbol{I}_n \cdot \boldsymbol{I}_m}{2} \frac{m^* J^2}{(2\pi)^6} P \iint_{\text{all occupied states}} \frac{J_0(K\rho_n) J_0(K'\rho_n')}{K^2 + \beta_2^2 - K'^2 - \beta_2'^2}$$
$$\times \frac{\psi^*(\beta_2, z_n)\psi(\beta_2, z_m)\psi(\beta_2', z_n)\psi^*(\beta_z', z_m)}{K^2 + \beta_2^2 - K'^2 - \beta_2'^2}$$
$$\times K'\, dK'\, K\, dK\, dk_z'\, dk_z$$

where $\boldsymbol{K}, \boldsymbol{K}'$, $\boldsymbol{\rho}_n$ and $\boldsymbol{\rho}_n'$ are 2D vectors, $\boldsymbol{\rho}$ being the vector distance of the projection onto the x–y plane of the distance between the atomic sites n and m and $z = z_n - z_m$ the distance in the z direction between these two sites. By choosing one of the sites (m) to be on the z axis and the other (n) to be in the x–y plane so that $z_n = 0$, $\rho_n^2 = x_n^2 + y_n^2$,

$x_m = y_m = 0$, and remembering that the form of $\psi(\beta_2, z)$ is $A(\beta_2)\exp(i\beta_2 z) + B(\beta_2)\exp(-i\beta_2 z)$, the following expression is obtained:

$$-2\pi^3 \frac{\boldsymbol{I}_n \cdot \boldsymbol{I}_m}{2} \frac{m^* J^2}{(2\pi)^6} \int_{\beta_{2\min}}^{\beta_{2F}} \int_0^{K_F} \frac{1}{R} J_0(K\rho_n) \cos(\beta_2' R)$$
$$\times [A_n(\beta_2') + B_n(\beta_2')][A_m^*(\beta_2') + B_m^*(\beta_2')]$$
$$\times [A_n^*(\beta_2) + B_n^*(\beta_2)][A_m(\beta_2)\exp(i\beta_2 z_m) + B_m(\beta_2)\exp(-i\beta_2 z_m)]$$
$$\times \frac{dk_z'}{d\beta_2'} \frac{dk_z}{d\beta_2} K\, dK\, d\beta_2 \tag{3}$$

where $R = \sqrt{\rho_n^2 + z_m^2}$, $\beta_2' = \sqrt{K^2 + \beta_2^2}$ and $dk_z/d\beta_2$, $dk_z'/d\beta_2'$ are related to γ and γ' by

$$dk_z/d\beta_2 = (\beta_2/\gamma)[af'(\gamma a)/(N + M)(a + b)\sqrt{1 - [f(\gamma a)]^2}]$$
$$dk_{z'}/d\beta_2' = (\beta_2'/\gamma')[af'(\gamma' a)/(N + M)(a + b)\sqrt{1 - [f(\gamma' a)]^2}]$$

with

$$f(\gamma a) = \cos[k_z(N + M)(a + b)]$$
$$f'(\gamma a) = -[(N + M)(a + b)/a]\sin[k_z(N + M)(a + b)](dk_z/d\gamma)$$

and the appropriate energy dependence is obtained from (2).

Equation (3) enables the RKKY coupling between the spins at sites n and m to be computed. All the expressions in the integrand can be determined from equations (1) and (2) using appropriate numerical techniques.

6. Magnetic ordering

If we write the energy of interaction between the spin at site n in plane n_0 and that at site m situated on the z axis in plane m_0 as

$$H''(x) = G\boldsymbol{I}_n \cdot \boldsymbol{I}_m F_{nm}$$

where

$$G = -2\pi^3[m^* J^2/(2\pi)^6][a^2/2(N + M)^2(a + b)^2]$$

then, in order to determine the type of magnetic ordering within a magnetic multiplane layer, we need to sum the interactions between each individual spin in a plane n_0 with the spin on the z axis in plane m_0 for all planes. The moment components for the various magnetic configuration can be described in terms of a wavevector $\boldsymbol{q}$ parallel to the c axis (z axis) giving the periodicity of moments in successive hexagonal planes, and a polar angle θ giving the moment orientation with respect to the c axis such that, for a spin $\boldsymbol{I}_i$ situated at $\boldsymbol{r}_i$,

$$I_{iz} = I\cos\theta$$
$$I_{ix} = I\sin\theta\cos(\boldsymbol{q} \cdot \boldsymbol{r}_i)$$
$$I_{iy} = I\sin\theta\sin(\boldsymbol{q} \cdot \boldsymbol{r}_i).$$

For general θ and $\boldsymbol{q}$ these expressions describe a conical moment arrangement. In our calculation we restrict the moments to lie in the hexagonal planes so that $\theta = \pi/2$, $I_{iz} = 0$. Hence, for the spins $\boldsymbol{I}_n$, $\boldsymbol{I}_m$ at $\boldsymbol{r}_n$ and $\boldsymbol{r}_m$,

$$\boldsymbol{I}_n \cdot \boldsymbol{I}_m = I^2 \cos(\boldsymbol{q} \cdot \boldsymbol{r}_{nm})$$

where $\boldsymbol{r}_{nm} = \boldsymbol{r}_n - \boldsymbol{r}_m$. The dot product in parentheses gives the turn angle between moments in successive planes. Because all the moments within any one plane are parallel, we can replace $\boldsymbol{r}_{nm}$ by $\boldsymbol{r}_{n_0 m_0}$, which is the distance between planes n_0 and m_0. Hence

$$H''(\boldsymbol{r}) = \sum_{m_0} \sum_{\text{all sites } n \text{ in plane } n_0} GF_{nm} I^2 \cos(\boldsymbol{q} \cdot \boldsymbol{r}_{n_0 m_0}) = GI^2 \sum_{m_0} F'_{n_0 m_0} \cos(q r_{n_0 m_0})$$

where

$$F'_{n_0 m_0} = \sum_{\text{all sites } n \text{ in plane } n_0} F_{nm}$$

is the interaction of all the moments on plane n_0 with the single moment on the z axis in plane m_0.

Thus, for the magnetic layer with four atomic planes,

$$\begin{aligned} H''(\boldsymbol{r}) = GI^2 \{ & (F'_{12} + F'_{21} + F'_{23} + F'_{32} + F'_{34} + F'_{43}) \cos[q(a+b)] \\ & + (F'_{13} + F'_{31} + F'_{24} + F'_{42}) \cos[2q(a+b)] \\ & + (F'_{14} + F'_{41}) \cos[3q(a+b)] \}. \end{aligned}$$

This will be a minimum when either

$$\sin[q(a+b)] = 0$$

or

$$\begin{aligned} & (F'_{12} + F'_{21} + F'_{23} + F'_{32} + F'_{34} + F'_{43}) \\ & \quad + 4(F'_{13} + F'_{31} + F'_{24} + F'_{42}) \cos[q(a+b)] \\ & \quad + 3(F'_{14} + F'_{41}) \{ 4 \cos^2[q(a+b)] - 1 \} = 0. \end{aligned}$$

The first case refers to either a ferromagnetic ($q = 0$) arrangement of all the moments on all four planes or an antiferromagnetic ($q = \pi/(a+b)$) alignment on alternate planes, whereas the second case can lead to a spiral configuration. It depends on which of the q-values makes $H''(r)$ the lowest in energy to determine the low-temperature ground-state configuration. Once the ordering of the four magnetic planes of the chosen unit cell has been established, the next step is to see how this ordering affects the associated ordering in the magnetic layers immediately adjacent to it through the long-range RKKY exchange interaction. From energy considerations we can establish the relative orientation of the spins in the nearest planes in the neighbouring cells; the arrangement of the moments on the other planes within these layers will be as determined above. We again need to consider the effect only on the spin sites on the z axis since it will be the same on any other spin on that plane. On the assumption that this spin is oriented at an angle θ with respect to the spins in the first atomic plane of the previous magnetic layer (which is always taken to be at $\theta = 0$ whatever the magnetic ordering of the layer as a whole may be), Then in general the energy of interaction between all the moments on

Table 1. Three magnetic layers ($M = 3$): AFM, antiferromagnetic; FM, ferromagnetic; S, spiral. The orderings for $N = 4$, 8 and 16 are in-phase correlations, and those for $N = 6$ and 12 are out-of-phase correlations.

N	4	6	8	10	12	14	16
Ordering	AFM	FM	FM	S	AFM	S	FM

Table 2. Four magnetic layers ($M = 4$): S, spiral; FM, ferromagnetic. The ordering for $N = 15$ is an in-phase correlation, and that for $N = 11$ is an out-of-phase correlation.

N	3	5	7	9	11	13	15	17
Ordering	S	S	S	S	FM$^-$	S	FM$^+$	S

all four planes of the previous magnetic layer with that single spin situated at site m' is given by

$$H''(r) = GI^2\{F'_{1m'}\cos\theta + F'_{2m'}\cos[q(a+b)+\theta] + F'_{3m'}\cos[2q(a+b)+\theta] + F'_{4m'}\cos[3q(a+b)+\theta]\}.$$

When the four magnetic planes are ferromagnetically aligned, then this is

$$GI^2(F'_{1m'} + F'_{2m'} + F'_{3m'} + F'_{4m'})\cos\theta$$

while for the antiferromagnetic case it is

$$GI^2(F'_{1m'} - F'_{2m'} + F'_{3m'} - F'_{4m'})\cos\theta.$$

This means that θ will be 0 or π depending on the sign of the term in parentheses. However, when a spiral arrangement exists in the magnetic layer, θ is given by

$$\tan\theta = -\{F'_{2m'}\sin[q(a+b)] + F'_{3m'}\sin[2q(a+b)] + F'_{4m'}\sin[3q(a+b)]\}/\{F'_{1m'} + F'_{2m'}\cos[q(a+b)] + F'_{3m'}\cos 2q(a+b)] + F'_{4m'}\cos[3q(a+b)]\}.$$

Similar but simpler expressions for $H''(r)$ and θ hold for the superlattice with three magnetic planes; terms involving the subscript 4 are omitted. The predicted ordering has been determined for systems containing 3–17 planes of the non-magnetic element intervening between either three or four magnetic planes.

The results are shown in tables 1 and 2. It can be seen from these data that changing the width of the magnetically inert layer does affect the type of ordering which is predicted to occur within the magnetic layers. For the case $M = 3$ (shown in table 1), ferromagnetic, antiferromagnetic and spiral ordering within the layers are all predicted within the relatively small range of values of N. For $M = 4$ (table 2), the predictions are mostly for spiral ordering, but ferromagnetic ordering also occurs.

It is known from the experimental data that any ordering within individual magnetic layers may be correlated across the non-magnetic region. For the ferromagnetic and antiferromagnetic orderings this occurs with almost equal occurrence of the in-phase and out-of-phase correlations. It is surprising that the insertion of only two layers of

non-magnetic material may alter radically the type of ordering predicted. Also it may leave the ordering unchanged but with the longer-distance correlations altered. No cases in which spiral ordering was continued coherently across the gap occurred, although in one or two cases the deviation in angle is quite small.

Overall this relatively simple model does show a variety of magnetic orderings similar to those seen in measurements made on magnetic superlattices. It appears likely that the RKKY interaction, which so dominates the properties of the RE metals and alloys, provides a critical element also in the behaviour of these superlattice systems.

7. Conclusions

The unit cells of most magnetic superlattices which have been investigated experimentally contain an extremely large number of sites. Because of this, any accurate and self-consistent 3D band-structure calculation would require enormous computing power, so that it is necessary to start any comparative analysis of theoretical and experimental data with band structures calculated from relatively simple models. The calculations reported in this paper are based on what is probably the simplest, but still realistic, model for dealing with systems in which the unit cell may contain more than 20 atoms.

Any calculation of the form of the RKKY interaction, and in particular its variation with distance, depends strongly on the band structure (both energies and wavefunctions) of the electrons. Results such as those presented in tables 1 and 2 indicate clearly that our simple model does produce a form of the RKKY interaction which permits the wide variety of magnetic orderings seen experimentally. By choosing the appropriate states of the two constituent elements in the superlattice to have energies with approximately the same binding, the overall electronic charge density within the unit cell is uniform and there is no charge transfer within the system. Of course, as indicated in figures 2 and 3, this does not imply that every state in a band corresponds to a uniform charge distribution and it can be surmised also that, if the conduction electrons are spin polarised when the system orders magnetically, it is possible that there will then exist within the so-called magnetically inert layers a spatial variation in the contribution by the electrons to the magnetism. Such an effect could produce spin-density waves which would have a direct bearing on the coherence of the magnetic ordering within the systems.

While the model has exhibited many of the features which magnetic superlattices have shown experimentally it does not suggest that spiral orderings (when they occur) should be as strongly coherent as they are. It may be that the inclusion of spin polarisation of the electrons is important for explaining this phenomenon. It may be also that the analysis must be more properly three dimensional. The existing calculations are being extended to include both of these aspects as realistically as is feasible. The successes of the simple model reported here encourages the belief that such extended computations could prove to have predictive value. Larger numbers of magnetic layers in each bilayer also can be treated and the rather more complicated analysis of which magnetic orderings may be expected will be published in a later paper.

References

Borchers J, Sinha S, Salamon M B, Du R, Flynn C P, Rhyne J J and Erwin R W 1987 *J. Appl. Phys.* **61** 4049–51

Cooper B R 1972 *Magnetic Properties of Rare Earth Metals* ed R J Elliott (New York: Plenum) pp 17–26
Kittel C 1963 *Quantum Theory of Solids* (New York: Wiley) pp 360–4
Hong M, Fleming R M, Kwo J, Schneemayer L F, Waszczak J V, Mannaerts J P, Majkrzak C F, Gibbs D and Bohr J 1987 *J. Appl. Phys.* **61** 4052–4
Majkrzak C F 1989 *Physica* B **156–7** 619–26
Majkrzak C F, Cable J W, Kwo J, Hong M, McWhan D B, Yafet Y, Waszczak J V, Grimm H and Vettier C 1987 *J. Appl. Phys.* **61** 4055–7
Majkrzak C F, Gibbs D, Boni P, Goldman A I, Kwo J, Hong M, Hsieh T C, Fleming R M, McWhan D B, Yafet Y, Cable J W, Bohr J, Grimm H and Chien C L 1988 *J. Appl. Phys.* **63** 3447–52
Rhyne J J, Erwin R W, Borchers J, Sinha S, Salamon M B, Du R and Flynn C P 1987 *J. Appl. Phys.* **61** 4043–8
Rhyne J J, Erwin R W, Borchers J, Salamon M B, Du R and Flynn C P 1989 *Physica* B **159** 111–28